AIP | Journal of Applied Physics

Cation and magnetic orders in MnFe2O4 from density functional calculations

Jhih-Rong Huang and Ching Cheng

Citation: J. Appl. Phys. 113, 033912 (2013); doi: 10.1063/1.4776771
View online: http://dx.doi.org/10.1063/1.4776771
View Table of Contents: http://jap.aip.org/resource/1/JAPIAU/v113/i3
Published by the AIP Publishing LLC.

JOURNAL OF APPLIED PHYSICS **113**, 033912 (2013)

Cation and magnetic orders in $MnFe_2O_4$ from density functional calculations

Jhih-Rong Huang and Ching Cheng[a)]
Department of Physics, National Cheng Kung University, Tainan 70101, Taiwan

(Received 28 June 2012; accepted 2 January 2013; published online 18 January 2013)

$MnFe_2O_4$ generally crystallizes in a mixed phase consisting of both the normal and inverse spinel structures with the fitted experimentally determined saturation moments of 5 and 3 μ_B per formula, respectively. Employing the density-functional methods with the generalized gradient approximation for the exchange-correlation energy functional and the on-site Coulomb effect (GGA+U), we have studied this material through exploring various cation distributions and magnetic orders of the system. We demonstrate that the magnetic moment can be accounted for by the high-spin Mn^{2+} cations at the tetrahedral site in the normal spinel structure and by the intermediate-spin Mn^{2+} cations at the octahedral site in the inverse spinel structure. That is, the results support the single-valence state for this material. The corresponding energetics, exchange interactions, and electronic properties are also presented and discussed. © *2013 American Institute of Physics*. [http://dx.doi.org/10.1063/1.4776771]

I. INTRODUCTION

Manganese ferrite, $MnFe_2O_4$ (MFO), is one of the iron spinels which are widely used in the microwave and magnetic recording applications characterized by high impedance and low core loss.[1] Recent applications of MFO include cancer detection via magnetic resonance imaging and promising cancer remediation therapy like drug delivery using MFO nanoparticles.[2] The structure of the spinel group is commonly categorized into normal and inverse spinel structures, according to the distribution of the divalent and trivalent cations filling the tetrahedral and octahedral sites (denoted as A and B sites, respectively, hereafter) in the fcc sublattice of oxygen. A normal spinel corresponds to the structure with all the A sites being occupied by the divalent cations and the B sites by the trivalent cations, e.g., $ZnFe_2O_4$ (ZFO) and $CdFe_2O_4$ (CFO). In an inverse iron spinel, the divalent cations occupy half of the B sites while the other half as well as all the A sites are occupied by the Fe ions, e.g., $NiFe_2O_4$ (NFO). Unlike the pure normal spinel materials, such as ZFO and CFO, and the inverse ones, such as NFO, MFO generally crystallizes in a mixed phase consisting of both the normal and inverse spinel structures. Consequently the chemical formula is usually represented by $(Mn_{1-\delta}Fe_\delta)[Fe_{2-\delta}Mn_\delta]O_4$, where δ is the inversion parameter. The round and square brackets denote the cations occupying the A and B sites, respectively. Depending on the material preparation, the δ in MFO nanoparticles can reach up to 67% while the most frequently observed δ in bulk MFO is 20%.[3,4]

In addition to the particular partial inversion in the cation distribution, there is also the not-yet-settled issue of the magnetic property, and accordingly the electronic valences of cations in MFO. MFO is a ferrimagnetic material whose dominant interaction is inferred as antiferromagnetic between the magnetic ions at A and B sites.[5–7] The interactions among B-site cations are believed to be also antiferromagnetic but much weaker which, together with the strong A-B antiferromagnetic interactions, would lead to parallel magnetic order among B-site cations to optimize the system's energy.[8,9] Usually, the exchange interactions between cations are analyzed by using the Heisenberg model: $H = -\sum_{i>j} J_{ij} S_i \cdot S_j$ where J_{ij} is the exchange interaction and the indices i and j denoting the cations at the *ith* and *jth* site. The experimentally determined saturation moments for the MFO single crystals with different degrees of inversion fit reasonably well into the formula of $5(1-\delta)+3\delta$.[10] That is, it supports the assignment of 5 and 3 μ_B/fu ($\mu_B/formula$) for the normal and inverse spinel structure of MFO, respectively.

The spin structure (if the orbital moments are negligible as concluded in the previous study[11]) for the normal spinel structure is commonly presumed as collinear with antiparallel magnetic order between the Mn (A site) and Fe (B site) cations, both contributing 5 μ_B, but parallel magnetic order among the Fe cations. However, there are two different models frequently adopted for the magnetic order of the inverse spinel structure.[10] One is a collinear model supported by nuclear magnetic resonance (NMR) experiments with magnetic moment of 5 μ_B for the Fe^{3+} ions at A site and 4 μ_B for both the Fe^{2+} and Mn^{3+} ions at B site.[12] The other is a canted model proposed from the results of Mössbauer experiments as only minute quantity of Fe^{2+} ions was detected.[7,10] The proposed Mn^{2+} ions at B site were assumed canting about 53° to the Fe^{3+} ions at B site, which are antiparallel to the moments of Fe^{3+} at A site, and contribute a total of 3 μ_B/fu to the inverse phase of the material. There is also experimental observation of a 10° deviation of B-site Fe cations from collinearity.[3] In addition to the unsettled magnetic configuration in the inverse phase, the cation distribution at B sites offers another degree of freedom in generating the possible structure of MFO, not to mention those due to the degree of inversion. These all make MFO a complex material.

In the present article, MFO with various cation distributions and magnetic orders are studied by the density

a)Electronic address: ccheng@mail.ncku.edu.tw.

functional theory (DFT)[13] based calculations. We shall demonstrate that a collinear model in magnetism can lead to the saturation moment consistent with experimental observations. The corresponding studies in energetics, magnetic, structural, and electronic properties will also be discussed in detail.

II. CALCULATION METHODS AND CONSIDERED STRUCTURES

In this study, all electronic calculations are based on the spin polarized DFT.[13] The plane-wave-based Vienna *ab initio* simulation program (VASP), which was developed by the Institute fu°r Material Physik of the Universität Wien, is used to calculate the electronic properties of MFO.[14] The interaction between ions and valence electrons is described by the projector augmented wave (PAW) method[15] which was implemented by Kresse and Joubert.[16] The valence electrons included are 7, 8, and 6 for Mn, Fe, and oxygen, respectively. The generalized gradient approximation (GGA) developed by Perdew, Burke, and Ernzerhof (PBE) is used for the exchange-correlation energy functional.[17]

For the transition-metal elements, the DFT+U approach is employed to cover the strong correlation of the d-orbital electrons.[18] This scheme incorporates a spherically averaged Hubbard parameter U for the on-site Coulomb interaction in the localized d orbitals and a parameter J for the screened exchange energy into the original DFT methods. The J values were shown to be only weakly dependent on the valence configuration[19] and in this study the values of 0.89 eV and 0.70 eV are used for Fe and Mn, respectively. The values of U can be calculated by the *ab initio* method developed previously.[20] Instead, we use an extensive range of U_{Mn} values, i.e., 0 (in this case, J_{Mn} is also taken as 0), 2, 4, and 7 eV, to explore the effect of the on-site Coulomb repulsion of Mn in MFO.[21] The strong correlation effect of Fe in iron spinels has been well established previously in the LDA+U scheme[11,22] as $U_{Fe}=4.5$ eV. This value is used in the present consideration, though the previous study of LDA+U with $U_{Mn}=4$ eV did not predict the experimentally observed insulating state.[23] It has been shown that GGA is superior to LDA in the DFT+U schemes as a modest value of U is sufficient to predict the closer to experimental volume and magnetic property of the studied material.[24] As it will be shown later that all the considered MFO phases in the present study with the non-zero U_{Mn} and 4.5 eV for U_{Fe} lead to insulating state. In the literature, the values of U_{Fe} used with GGA+U vary from 2.5 eV (Ref. 25) to 5.5 eV (Ref. 26). Finally, we should mention that another approximation assumed in this study is that a set of fixed values of U and J are used for both the normal and inverse spinel structures as well as the different magnetic configurations which have different symmetries.

All the self-consistent calculations are converged until the total energy difference between electronic iterations being smaller than 10^{-4} eV per cubic cell (8 formulas, i.e., 56 atoms). The energy cutoff that determines the number of plane waves is 500 eV, and the k-point sampling according to Monkhorst-Pack[27] used is $(6\times6\times6)$. Atomic relaxation is implemented until the atomic forces are less than 0.02 eV/Å and the cell volume is also relaxed while keeping the unit cell in cubic symmetry. Tests on higher energy cutoff (600 eV) and denser Mohkhorst-Pack mesh of $(8\times8\times8)$ show that the energy differences between the lowest-energy phases of the normal and inverse spinel MFO (around 100 meV/*fu*) are converged to within 1 meV/*fu*.

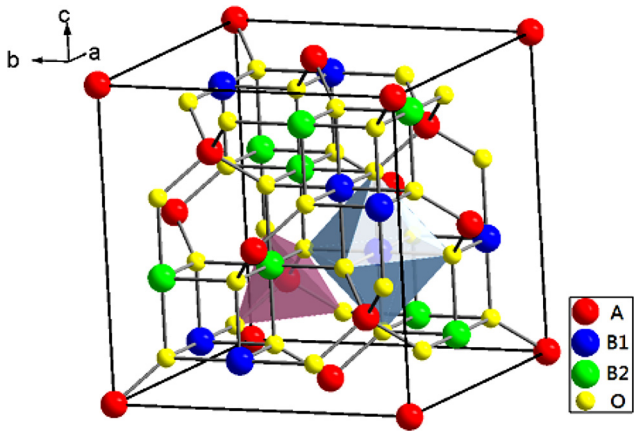

FIG. 1. The cubic unit cell consisting of eight formulas used in the calculations. Here shows the SC3 configuration for the distribution of the two groups of cations at B sites. A representative tetrahedron around the A-site cation and octahedron around the B-site cation are also presented.

Throughout this study, cubic unit cell consisting of eight MFO formula units is used in order to investigate the ionic and magnetic interactions between cations (Fig. 1). Four different distributions for the equally divided two groups of cations (or spin configurations) at B sites (denoted as B1 and B2 hereafter) are considered as in the previous study for ZFO (Fig. 1 of Ref. 28) and are numbered as structures SC1 to SC4. Both the cation arrangements and magnetic orders can be generated according to the four distributions. The structures of MFO are denoted as, e.g., I3pnn, for inverse spinel structure and the number 3 indicates that the distribution of cations (spin configurations) at B site is according to the SC3 distribution. Their corresponding distributions of cations and magnetic orders are listed in Table I. Note that there is no distinction between the different cation distributions of SC1 to SC4 for both Npnn and Nppp as the B1 and B2 sites are occupied by the same cation (Fe) in these two phases. The lattice constants for all the studied phases,

TABLE I. The notation, with the corresponding cation distributions and magnetic orders, used for the phases considered in this study. The magnetic orders are represented by the parallel (++ or −−) or antiparallel (+−) magnetic moments between the cations. For example, Npnn is normal spinel with positive A, negative B1, and negative B2 spin states while I3pnp is inverse spinel with positive A, negative B1, and positive B2 spin states. The number 3 in I3pnp indicates that the distribution of cations (spin configurations) at B site in this structure is according to the SC3 distribution (details in Sec. II).

	Normal spinel				Inverse spinel				
site	ion	Npnn	Nppp	N3pnp	ion	I3pnn	I3ppp	I3pnp	I3ppn
A	Mn	+	+	+	Fe	+	+	+	+
B1	Fe	−	+	−	Fe	−	+	−	+
B2	Fe	−	+	+	Mn	−	+	+	−

TABLE II. The calculated total energies of the studied normal and inverse spinel phases at different U_{Mn} relative to the phase Npnn. The number in the structure notations indicates the distribution of cations (spin configurations) at B site, e.g., 4 for SC4 (details in Sec. II).

eV	Normal spinel (eV/*fu*)						Inverse spinel (eV/*fu*)			
U_{Mn}	Npnn	Nppp	N3pnp	N1pnp	N2pnp	N4pnp	I3pnn	I3ppp	I3pnp	I3ppn
0	0	1.047	0.562	0.567	0.535	0.460	−0.112	0.329	0.165	−0.069
2	0	0.736	0.326	0.340	0.335	0.328	0.100	0.565	0.156	0.150
4	0	0.539	0.217	0.234	0.235	0.220	0.126	0.791	0.424	0.457
7	0	0.361	0.120	0.137	0.138	0.124	0.032	0.781	0.234	0.427

irrespective of the U_{Mn} values, are found to be all within 2% deviation as compared to the experimentally reported room-temperature value of 8.511 Å.[29]

III. ENERGETICS

The most stable normal and inverse spinel structures are identified as the Npnn and I3pnn, respectively, regardless of the size of the on-site Coulomb interactions U_{Mn} for Mn considered in this study (Table II). Besides, the Npnn phase is more stable than I3pnn, except in the $U_{Mn}=0$ case whose most stable structure is the inverse I3pnn. Note that, as discussed in the introduction, the dominant contribution observed experimentally in the mixed phase of bulk MFO is the normal spinel structure. This result, therefore, suggests the essential inclusion of the on-site Coulomb interaction of Mn cation in this material. The $U_{Mn}=0$ case is not included in the following discussion, unless specified explicitly. The Npnn phase is more stable than the I3pnn by, at most, 0.13 eV/*fu*. This is noticeably smaller than the corresponding energy difference of 0.8 eV/*fu* (the smallest energy difference among all the considered U_{Ni} cases) for the inverse spinel material of NFO[30] and 0.21 and 0.35 eV/*fu* for the normal spinel materials of ZFO and CFO.[28] These results are in parallel with the formation of MFO mixed phase through the small energy difference between the normal and inverse spinel phases and the commonly observed 20% inversion parameter through the outcome that the normal spinel phase is the more stable one.

For the normal spinel structures, the magnetic order of the Mn(A), Fe(B1), and Fe(B2) cations alone predominantly determines the relative stability among different phases, i.e., the energy differences with the same magnetic order of the Mn(A), Fe(B1), and Fe(B2) cations but different B-site magnetic distributions are minute. In other words, the total energies of N1pnp, N2pnp, and N4pnp are little different from that of N3pnp (Table II). This suggests the much smaller exchange interactions among the B-site Fe cations when compared to the exchange interaction between the A-site Mn and B-site Fe cations. As the on-site Coulomb effect of Mn cations increases, the energy differences (with respect to the energy of the lowest-energy phase Npnn) decrease which implies a decreasing exchange interactions between cations. The exchange interactions will be discussed in Sec. V.

Concerning the inverse spinel structures, the magnetic order of the Fe(A), Fe(B1), and Mn(B2) cations as well as the distributions of the B1 and B2 sites are both important factors in energetics. For the phases with the same magnetic order for the A, B1, and B2 cations in the inverse spinel structure, the SC3 distribution was found to be more stable than the SC1, SC2, and SC4 ones. The energy differences are more than 70 meV/*fu*. Similar conclusion that the SC3 distribution is the most stabilized one was also found in the NFO system.[30] Consequently the following discussions will focus on the structures with the SC3 distribution for the B1-site(Fe) and B2-site(Mn) cations. The results of inverse spinel phases with SC3 distribution are listed in Table II. The most stable inverse spinel structure is the I3pnn phase, irrespective of the considered U_{Mn} values. The energy differences do not show the similar monotonic behavior with respect to the on-site effect of the (B2-site) Mn cations as those in the normal spinel phases. We shall see that this is closely related to the changes in magnetic behavior as U_{Mn} varies in the inverse spinel phases.

IV. MAGNETIC MOMENTS AND CATION VALENCES

The calculated total magnetic moments of the studied phases are listed in Table III. The magnetic moments for all the normal phases are independent of the U_{Mn} values, except in the $U_{Mn}=0$ case, and can be accounted for by the equally contributed local moment of 5 μ_B from all the cations. However, the magnetic moment for the inverse spinel phases depend on the on-site Coulomb effect of Mn. For the lowest-energy inverse spinel phase, i.e., I3pnn, the moments for the A-site Fe and B1-site Fe are antiparallel and have the same magnitude, i.e., they cancel each other out. The total moment of I3pnn is, therefore, determined solely by the moment of the B2-site Mn cations. In the cases of $U_{Mn}=2$ eV, the B2-site Mn cations contribute 3 μ_B (referred to as intermediate-spin state hereafter), though a 5 μ_B (referred to as high-spin state hereafter) is found in the cases of higher U_{Mn} values. Analyses of the partial density of states (PDOS) show that, as U_{Mn} is increased from 2 to 4 eV, the e_g orbital in the majority spin component locating above the Fermi level (E_F) moves down to become one the occupied states while the originally, i.e.,

TABLE III. Total magnetic moment of the studied phases at different U_{Mn}.

eV	Nomal spinel (μ_B/*fu*)			Inverse spinel (μ_B/*fu*)			
U_{Mn}	Npnn	Nppp	N3pnp	I3pnn	I3ppp	I3pnp	I3ppn
0	5	11	3	3	11	3	5
2	5	15	5	3	13	3	5
4	5	15	5	5	13	5	5
7	5	15	5	5	15	5	5

in the $U_{Mn}=2$ eV case, occupied e_g orbital in the minority spin component is pushed up above E_F to become unoccupied (Fig. 2(a)). In other words, the majority and minority components of the spin-polarized e_g orbitals for Mn^{2+} cations are shifted relative to each other depending on the U_{Mn} values to result in different magnetic moments while at the same time maintain in the same valence. Similar change takes place in I3pnp with the same reason.

These U_{Mn}-dependent changes in magnetic configurations are closely associated with the relaxed structures of the phases. In the $U_{Mn}=2$ eV case, we are able to generate the metastable high-spin states for I3pnn and I3pnp with magnetizations of $5\,\mu_B/fu$. Their total energies are about 90 and 450 meV/fu higher than the corresponding intermediate-spin states of I3pnn and I3pnp listed in Table III, respectively. They are obtained from treating the relaxed I3pnn and I3pnp structures of the $U_{Mn}=4$ eV case as the initial atomic positions and carrying out the structural relaxation using $U_{Mn}=2$ eV. The major differences between the intermediate-spin and high-spin structures are the smaller nearest-neighbor Mn-O bonds (around 1.92 Å as compared to those around 2.13 Å) and accordingly the larger Fe(B1)-O-Mn(B2) angles (around $94°-97°$ as compared to $91°-93°$) in the intermediate-spin structures. That is, the octahedra formed by the nearest-neighbor oxygen ions around Mn cations are considerably smaller in the intermediate-spin I3pnn than those in the high-spin I3pnn. Note that the present result is a close resemblance to the 0.16 Å difference in ionic radii for the intermediate-spin and high-spin Mn^{2+} in octahedral environment, i.e., 0.81 and 0.97 Å respectively.[31] However, the magnetic moments contributed by the A-site Mn cations in the normal spinel structures do not have this U_{Mn}-dependent behavior, the contribution is always found to be $5\,\mu_B/fu$. One also notices that the d electrons of Fe cations are strongly localized in the Npnn phase for both $U_{Mn}=2$ and 4 eV cases as well as in the $U_{Mn}=4$ eV case of I3pnn; but not in the $U_{Mn}=2$ eV case of I3pnn (Figs. 2(b) and 2(c)).

The experimental observations support the assignment of 5 and $3\,\mu_B/fu$ for the normal and inverse spinel structure of

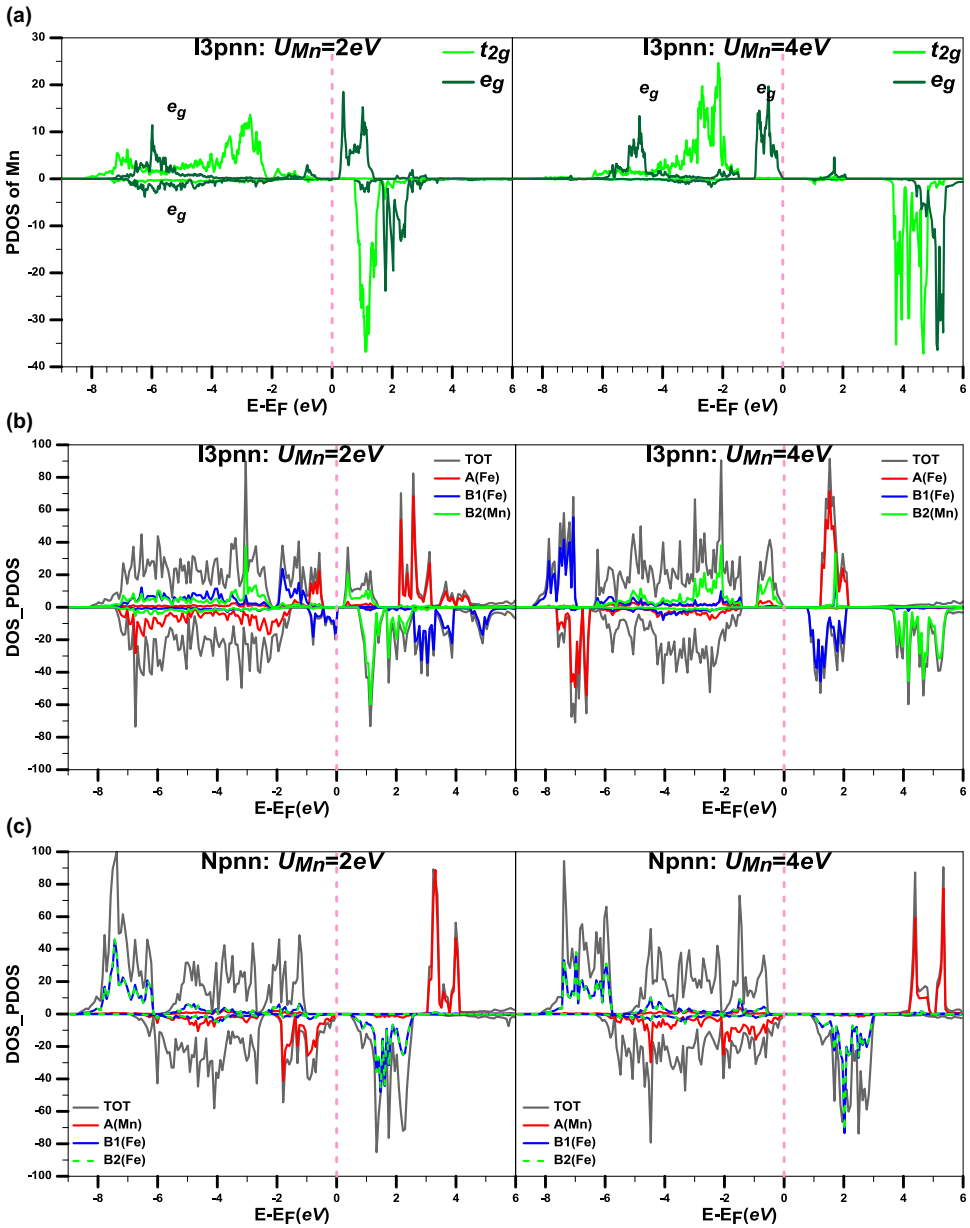

FIG. 2. (a) The e_g and t_{2g} partial density of states for the B2-site Mn cations in the I3pnn phase and the DOS and PDOS for the (b) I3pnn and (c) Npnn obtained with $U_{Mn}=2$ eV and $U_{Mn})=4$ eV.

MFO, respectively.[10] This would correspond to the case of $U_{Mn}=2$ eV (see Table IV). The $U_{Mn}=0$ case is excluded here due to the energetics consideration as discussed in Sec. III. The magnetization of these materials is usually treated by the ionic model whose local magnetic moment is determined by the Hund's rule for d orbitals. For example, the magnetic moments for the Fe^{2+}, Fe^{3+}, Mn^{2+}, and Mn^{3+} are assigned as 4, 5, 5, and 4 μ_B, respectively. However, the integration of the PDOS for the cations (sum of the majority and minority spin components) indicates that the electronic valence for B2-site Mn cations stays about the same as U_{Mn} values increase from 2 eV to 4 eV while at the same time the corresponding magnetic-moment changes from 3 to 5 μ_B/fu (Fig. 2(a)). That is, the electronic valence of Mn can be identified as d^5 (Mn^{2+}) in both the Npnn and I3pnn phases. This conclusion, i.e., supporting the single-valence state of Mn^{2+} in MFO, is consistent with the recent experiment,[32] though there is also previous experiment with non-conclusive result.[33]

V. EXCHANGE INTERACTIONS

The exchange interactions between cations are determined by applying the Heisenberg model: $H=-\sum_{i>j}J_{ij}S_i\cdot S_j$ to the evaluated total energies of the considered phases. For the normal spinel phases, the nearest-neighbour interaction (J_{1AB}) between the A-site (Mn) and B-site (Fe) cations and the first three neighboring interactions ($J_{1BB}, J_{2BB}, J_{3BB}$) among the B-site cations (Fe) are listed in Table IV. The J_{1AB} values can be obtained from the energies of Nppp and Npnn alone while the interactions among B-site Fe cations are from those of Nppp, Npnn, N1pnp, N2pnp, and N3pnp. Slightly different values of J_{BB}'s can be obtained from replacing N3pnp by N4pnp. The differences are no more than 0.1 meV, except in the $U_{Mn}=0$ case which will not be included in the following discussion as the energetic consideration does not favor its application.

For the normal spinel structures, all the interactions are found to be antiferromagnetic and the A-B exchange interaction is one order larger than those of the B-B exchange interactions. That is, the dominant interactions are between the A-site Mn and B-site Fe cations. The strong A-B interactions are mediated through the around 120° Mn-O-Fe angle whose connecting structure provides the strong coupling between d orbitals of the A-site Mn and B-site Fe cations via the p orbital of oxygen anions while, on the other hand, the B-B interactions are mediated through the around 95° Fe-O-Fe angle. Note that we have taken the local moment (5 μ_B) as one ($S_i=1$) in this analysis, i.e., the exchange interaction corresponds to half of the energy required to flip a local moment if only one neighbour is present.

TABLE IV. The exchange interactions for the normal and inverse spinel phases at different U_{Mn}.

eV	Normal spinel (meV)				Inverse spinel (meV)		
U_{Mn}	J_{1AB}	J_{1BB}	J_{2BB}	J_{3BB}	J_{AB1}	J_{AB2}	J_{B1B2}
0	−43.6	6.2	−0.3	−0.5	−8.7	−28.1	−7.5
2	−30.6	−2.8	−0.3	−1.1	−15.1	−15.5	−16.4
4	−22.5	−4.5	0.0	−1.0	−33.9	−31.2	−9.5
7	−15.0	−5.0	−0.1	−1.2	−39.2	−23.1	−9.5

With the total energies of the four magnetic orders considered in this study for the inverse spinel phases, i.e., I3pnn, I3ppp, I3pnp, and I3ppn, three exchange interactions can be derived. They are all interactions between nearest neighbors, i.e., that between the A-site (Fe) and B1-site (Fe) cations (J_{AB1}), that between the A-site (Fe) and B2-site (Mn) cations (J_{AB2}), and that between the B1-site (Fe) and B2-site (Mn) cations (J_{B1B2}). All these three nearest-neighbor interactions are found antiferromagnetic. However, one notices that, for the case of $U_{Mn}=2$ eV, the J_{B1B2} interaction is at the same order of magnitude as those of J_{AB1} and J_{AB2} interactions. This is likely due to the around 10% smaller ionic radii of the intermediate-spin Mn^{2+} cations in the I3pnn, I3ppn, and I3pnp phases of the $U_{Mn}=2$ eV case. For these three phases, the corresponding Fe-O-Mn (B1-O-B2) angles change from about 91°–93° in the $U_{Mn}=4$ eV case to about 94°−97° in the $U_{Mn}=2$ eV.

In the inverse spinel phases, there is one more complication in evaluating the J values coming from the different local-moment contributions in the four considered inverse spinel phases for the cases of $U_{Mn}=2$ eV and $U_{Mn}=4$ eV. In the $U_{Mn}=7$ eV case, the local moment of 5 μ_B is treated as one ($S_i=1$) as in the normal spinel cases. Similar assignment is used in the $U_{Mn}=4$ eV case with the appropriate modifications of the coefficients (for J_{ij}) as the corresponding local moments in the I3ppp phase are 4, 5, and 4 μ_B for the A-site (Fe), B1-site (Fe), and B2-site (Mn) cations, respectively. In the $U_{Mn}=2$ eV case, the local moments of 4, 4, and 3 μ_B ($S_i=1$) are treated as one ($S_A=1, S_{B1}=1, S_{B2}=1$) for the A (Fe), B1(Fe) and B2(Mn) cations, respectively, with similar coefficient modifications for the I3ppp phase. However, the main conclusion that the J_{B1B2} interaction is at about the same magnitude as J_{AB1} and J_{AB2} in the $U_{Mn}=2$ eV case stays the same no matter whether the coefficients and the assignments of local moments are adjusted or not. The large antiferromagnetic exchange interactions between B1 (Fe) and B2(Mn) cations in the $U_{Mn}=2$ eV case are therefore closely linked to the intermediate-spin magnetic configuration of the Mn cations in the I3pnn (as well as I3pnp and I3ppn) phases.

VI. ELECTRONIC PROPERTIES

Inclusions of the on-site Coulomb interactions as considered in this study lead to insulating Nppp and N3pnp phases of MFO as shown in Table V. That is, the two phases are conductors for the $U_{Mn}=0$ case. The size of the band gaps depends on the magnetic order as well as the cation distribution. However, it increases with the size of U_{Mn} generally. In the $U_{Mn}=2$ eV case, whose magnetic moments for the lowest-energy normal and inverse spinel structures are consistent with the experimental observations of 5 and 3 μ_B/fu, respectively, the band gap is 0.47 eV for Npnn and 0.24 eV for I3pnn. These results closely resemble the conclusion of an early experimental study[34] which determined the band-gap value as 0.30 eV.

The exchange splitting, also listed in Table V, in the conduction bands is believed to be a determinant factor for

TABLE V. Band gaps and the exchange splittings in the conduction bands (numbers in parentheses) of the studied phases at different U_{Mn}.

E (eV)	Normal spinel			Inverse spinel			
U_{Mn}	Npnn	Nppp	N3pnp	I3pnn	I3ppp	I3pnp	I3ppn
0	0.18	0.00	0.00	0.25	0.12	0.37	0.60
	(2.04)	(0.00)	(0.00)	(0.17)	(0.31)	(0.02)	(0.19)
2	0.47	0.32	0.96	0.24	0.25	0.47	0.57
	(2.32)	(1.83)	(0.40)	(0.53)	(0.16)	(0.36)	(0.57)
4	0.91	0.74	1.44	0.79	0.58	0.89	0.42
	(2.29)	(1.76)	(0.29)	(0.46)	(0.28)	(0.07)	(2.06)
7	1.36	1.06	1.76	1.38	0.75	1.46	0.95
	(2.23)	(1.71)	(0.19)	(0.33)	(1.86)	(0.00)	(2.01)

the potential application of MFO as a spin filter. Similar to the previous theoretical study, we found the exchange splitting in the normal spinel phases much larger than those in the inverse spinel ones.[11]

VII. CONCLUSION

We have carried out DFT with GGA + U calculations to study the physical properties of $MnFe_2O_4$. The materials with various cation distributions and magnetic orders were explored with different on-site Coulomb effect for the d electrons of Mn cations. The most stable normal and inverse structures are identified as the Npnn and I3pnn phases, respectively, irrespective of the U_{Mn} values considered in this study. It was found that in the $U_{Mn} = 2$ eV case, the magnetic moments of both the Npnn and I3pnn phases are consistent with the experimental values of 5 and 3 μ_B/fu. The results support the single-valence state of Mn^{2+} for MFO, i.e., with the high-spin state of Mn^{2+} at the tetrahedral site in the normal spinel structure and the intermediate-spin state of Mn^{2+} at the octahedral site in the inverse spinel structure. The corresponding exchange interactions are derived and their connections with the relaxed structures are discussed. Finally, all the studied phases, except the Nppp and N3pnp phases in the $U_{Mn} = 0$ cases, were found having finite band gaps with larger exchange splitting in the normal spinel phases.

ACKNOWLEDGMENTS

This work was supported by the National Science Council of Taiwan. Part of the computer resources are provided by the NCHC (National Center of High-performance Computing). We also thank the support of NCTS (National Center of Theoretical Sciences) through the CMR (Computational Material Research) focus group.

[1]A. Goldman, *Modern Ferrite Technology* (Marcel Dekker, New York, 1993).
[2]J. Lee, J. Yang, H. Ko, S. J. Oh, J. Kang, J.-H. Son, K. Lee, S.-W. Lee, H.-G. Yoon, J.-S. Suh, Y.-M. Huh, and S. Haam, Adv. Funct. Mater. **18**, 258–264 (2008); *Scientific and Clinical Applications of Magnetic Carriers*, edited by U. Häfeli, W. Schütt, J. Teller, and M. Zborowski (Plenum, New York, 1997).
[3]J. P. Chen, C. M. Sorensen, K. J. Klabunde, G. C. Hadjipanayis, E. Devlin, and A. Kostikas, Phys. Rev. B **54**, 9288 (1996).
[4]M. H. Mahmoud, H. H. Hamdeh, J. C. Ho, M. J. O'Shea, and J. C. Walker, J. Magn. Magn. Mater. **220**, 139 (2000); M. Popa, P. Bruna, D. Crespo, and J. M. C. Morenoz, J. Am. Ceram. Soc. **91**, 2488 (2008).
[5]J. B. Goodenough, *Magnetism and the Chemical Bond* (Krieger, New York, 1976).
[6]A. J. Heeger and T. W. Houston, Phys. Rev. **135**, A661 (1964).
[7]G. A. Sawatzky, F. Van der Woude, and A. H. Morrish, Phys. Rev. **187**, 747 (1969).
[8]W. Wegener, D. Scheerlinck, E. Legrand, and S. Hautecler, Solid State Commun. **15**, 345 (1974).
[9]Xu Zuo and Carmine Vittoria, Phys. Rev. B **66**, 184420 (2002).
[10]Z. Simsa and V. A. M. Brabers, IEEE Trans. Magn. **11**(5), 1303 (1975).
[11]Z. Szotek, W. M. Temmerman, D. Kodderitzsch, A. Svane, L. Petit, and H. Winter, Phys. Rev. B **74**, 174431 (2006).
[12]H. Stepankova, B. Sedlak, V. Chlan, P. Novak, and Z. Simsa, Phys. Rev. B **77**, 092416 (2008).
[13]P. Hohenberg and W. Kohn, Phys. Rev. **136**, B864 (1964); U. von Barth and L. Hedin, J. Phys. C **5**, 1629 (1972); A. K. Rajagopal and J. Callaway, Phys. Rev. B **7**, 1912 (1973).
[14]G. Kresse and J. Hafner, Phys. Rev. B **47**, 558 (1993); **49**, 14251 (1994); G. Kresse and J. Furthmuller, *ibid.* **54**, 11169 (1996); Comput. Mater. Sci. **6**, 15 (1996).
[15]P. E. Blöchl, Phys. Rev. B **50**, 17953 (1994).
[16]G. Kresse and D. Joubert, Phys. Rev. B **59**, 1758 (1999).
[17]J. P. Perdew, K. Burke, and M. Ernzerhof, Phys. Rev. Lett. **77**, 3865 (1996).
[18]V. I. Anisimov, J. Zaanen, and O. K. Andersen, Phys. Rev. B **44**, 943 (1991); A. I. Liechtenstein, V. I. Anisimov, and J. Zaanen, *ibid.* **52**, R5467 (1995).
[19]I. V. Solovyev, P. H. Dederichs, and V. I. Anisimov, Phys. Rev. B **50**, 16861 (1994)
[20]M. Cococcioni and S. de Gironcoli, Phys. Rev. B **71**, 035105 (2005); V. L. Campo, Jr. and M. Cococcioni, J. Phys. Condens. Matter **22**, 055602 (2010).
[21]Claude Ederer and Matej Komelj, Phys. Rev. B **76**, 064409 (2007).
[22]V. I. Anisimov, I. S. Elfimov, N. Hamada, and K. Terakura, Phys. Rev. B **54**, 4387 (1996)
[23]V. N. Antonov, B. N. Harmon, and A. N. Yaresko, Phys. Rev. B **67**, 024417 (2003).
[24]A. Rohrbach, J. Hafner, and G. Kresse, J. Phys. Condens. Matter **15**, 979 (2003).
[25]S. Lebegue, S. Pillet, and J. G. Angyan, Phys. Rev. B **78**, 024433 (2008).
[26]M. Angst, P. Khalifah, R. P. Hermann, H. J. Xiang, M.-H. Whangbo, V. Varadarajan, J. W. Brill, B. C. Sales, and D. Mandrus, Phys. Rev. Lett. **99**, 086403 (2007).
[27]H. J. Monkhorst and J. D. Pack, Phys. Rev. B **13**, 5188 (1976).
[28]C. Cheng, Phys. Rev. B **78**, 132403 (2008).
[29]R. Vautier and M. Paulus, in *Landolt-Börnstein Numerical Data and Functional Relationships in Science and Technology*, new series, edited by K.-H. Hellwege (Springer, New York, 1970), Group III, Vol. 4, Part B, Chap. 6, p. 106, and references therein.
[30]C. Cheng, J. Magn. Magn. Mater. **325**, 144 (2013).
[31]See http://www.webelements.com for information about the ionic radii for the low-spin and high-spin Mn^{2+} in octahedral environment.
[32]S. Matzen, J.-B. Moussy, R. Mattana, K. Bouzehouane, C. Deranlot, F. Petroff, J. C. Cezar, M.-A. Arrio, Ph. Sainctavit, C. Gatel, B. Warot-Fonrose, and Y. Zheng, Phys. Rev. B **83**, 184402 (2011).
[33]J.-S. Kang, G. Kim, H. J. Lee, D. H. Kim, H. S. Kim, J. H. Shim, S. Lee, H. G. Lee, J. Y. Kim, B. H. Kim, and B. I. Min, Phys. Rev. B **77**, 035121 (2008).
[34]F. K. Lotgering, J. Phys. Chem. Solids **25**, 95 (1964).